Int. J. Electrochem. Sci., 17 **(2022)** Article Number: 220237, doi: 10.20964/2022.02.42

International Journal of
ELECTROCHEMICAL
SCIENCE
www.electrochemsci.org

Synthesis and Electrochemical Properties of NiO/Ni Composite as an Anode for Lithium-ion Batteries

Shuqiong Zhang[1,2,3,&], Qunfang Zhao[1,2,3,&], Chang Wang[1,2,3], Minyi Hu[1,2,3], Jianhua Ge[1,2,3], Xinai Yu[4], Guanghui Jiang[1,2,3,], Quansheng Ouyang[1,2,3,*]*

[1] Advanced Batteries and Materials Engineering Research Center, Guizhou Light Industry Technical College, Guiyang 550025, China;
[2] Graphene Materials Engineering Research Center of Guizhou Colleges and Universities, Guiyang 550025, China;
[3] Provincial Collaborative Innovation Center of Used Power Batteries Recycling, Guiyang 550025, China;
[4] Anhui Yufan Environmental Protection Technology Co., Ltd, Wuhu 241002, China;
& These authors contributed equally to this work and should be considered co-first authors
[*]E-mail: qsouyang@163.com

Received: 7 November 2021 / *Accepted:* 21 December 2021 / *Published:* 5 January 2022

NiO has been widely studied in the field of lithium-ion batteries because of its high theoretical capacity density (718 mAh g^{-1}), abundant raw materials, simple preparation methods and environmental friendliness. However, its poor conductivity as an electrode material still limits its practical application in batteries. In this paper, the Ni metal addition method is used to improve the conductivity of NiO. A Ni-based precursor is first prepared by the water bath method. The NiO/Ni composite with a flower-like structure was obtained by thermal decomposition of a Ni-based precursor in an argon atmosphere. The as-prepared NiO/Ni composite consists of sheet-like NiO and granular Ni, and the NiO content in the NiO/Ni composite is 52.7%. As the anode of a lithium-ion battery, the NiO/Ni composite electrode shows high capacity and a long cycle life with a capacity of 631.2 mAh g^{-1} at a current density of 0.5 A g^{-1} for the 100th cycle. It also exhibits excellent rate performance. The discharge capacities of the NiO/Ni composite are 671.2, 460.3, 376.1, 344.9 and 555.8 mAh g^{-1} at current densities of 0.5, 1, 2, 4 and 0.5 A g^{-1}, respectively. This explains why the NiO/Ni composite can endure a high charge-discharge current density. The results indicate that the NiO/Ni composite is a good anode material for lithium-ion batteries.

Keywords: NiO/Ni composite; Flower-like structure; Anode; Lithium-ion battery

1. INTRODUCTION

To meet the growing demand for electronic devices, it is necessary to develop a large number of low-cost, high-capacity and environmentally friendly energy storage devices [1]. Lithium-ion

batteries have the advantages of high energy density, high output voltage and good cycling performance [2-5] and are the most widely used energy storage devices.

At present, the main materials used as anode materials for lithium-ion batteries are carbon materials [6-8], metal oxides [9-18], silicon-based materials [19-22] and tin-based materials [23-24]. Compared with metal oxide materials, the reversible capacity of carbon materials is lower, and the vol ume change of silicon-based and tin-based materials is larger. Among these metal oxide materials, NiO has attracted much attention mainly because NiO has a high theoretical capacity density (718 mAh g^{-1}), abundance of raw materials, simple preparation, and environmental friendliness [25]. Despite these advantages, it still exhibits poor cycle stability due to the low conductivity of NiO. The electrons produced by the battery reaction are difficult to transmit in the material. There are many reported methods to solve the issue of poor conductivity. For example, NiO material can be grown directly on Cu foil [26] or Ni foam [27]. The barrier of poor conductivity can also be solved with cladding or loading carbon [28], with doping metals such as Co [29] and Ni [30-31]. Regarding the structure of NiO, many reports have focused on structural stability improvement, such as porous nanosphere structures [32-33] and nanotube structures [34], which have shown long cycling lives and high rate charge-discharge performances.

A flower-like structure of electrode materials has been reported frequently in recent studies for batteries[34-35]. Wu and co-workers constructed specific mesostructured NiO/Ni materials with flower-like structures for application in supercapacitors. The NiO/Ni electrode displayed excellent electrochemical performance because of its short solid state ion diffusion length, high electrolyte wettability and good conductivity[36]. This flower-like structure should also have the potential of excellent electrochemical performance when used in lithium-ion batteries.

In this work, a NiO/Ni composite with a hierarchical porous structure and flower-like morphology was prepared by calcining a nickel-based precursor in an argon atmosphere. For comparison, a NiO sample with a similar structure and morphology was synthesized by calcining the Ni-based precursor in air. Electrochemical tests of the as-prepared NiO/Ni and NiO as anodes for lithium-ion batteries showed that NiO/Ni has a high capacity and favourable cycle life. The results indicate that the NiO/Ni composite is a desirable anode material for lithium-ion batteries.

2. EXPERIMENTAL SECTION

2.1 Materials synthesis

The preparation method of Ni-based precursors and NiO/Ni composites is an uncomplicated procedure. Nickel nitrate (5.8 g, 20 mmol, $Ni(NO_3)_2{\cdot}6H_2O$) was dissolved in 100 mL distilled water under constant stirring at a constant temperature of 40 °C (in a round-bottomed flask). First, 2.8 g (20 mmol) of hexamethylenetetramine (HMT) and 0.2 g of oxalic acid dihydrate ($H_2C_2O_4{\cdot}2H_2O$) were dissolved in 10 mL distilled water to prepare a mixed solution which was added to the above nickel nitrate solution. Then, the green transparent mixture was heated to 95 °C (±5 °C) and the temperature was maintained for 6 h under normal pressure. After the reaction, the system was allowed to cool to

room temperature. The contents of the round-bottomed flask were washed three times with distilled water and ethanol separately and vacuum-dried at 60 °C to obtain a Ni-based precursor. Ar gas was pumped into a conventional atmospheric pressure chemical vapour deposition (CVD) reactor. Subsequently, the above Ni-based precursor was calcined at 335 °C for 2 h under an Ar atmosphere in a furnace. After cooling to room temperature, a NiO/Ni composite was obtained. For comparison, a pure NiO sample was obtained by calcining the above precursors in air at the same temperature.

2.2 Characterization

The NiO/Ni composite and the pure NiO sample were analysed by X-ray powder diffraction (XRD, Philips X'pert Pro ray diffraction). The structure and morphology of the two materials were characterized by scanning electron microscopy (SEM, S-4800) and transmission electron microscopy (TEM, JEM-100S). Their microstructures were characterized by high-resolution transmission electron microscopy (HRTEM). The content of metallic Ni was calculated from the weight loss of the reduction of NiO to Ni(0) in Ar/H_2 gas (10 vol% H_2) with a thermogravimetry analyser (STA-499F3 NETZSCH thermal analyser). The reaction is: $NiO + H_2 \rightarrow H_2O + Ni(0)$.

2.3 Electrochemical measurements

The preparation and electrochemical tests of the NiO/Ni material and NiO sample as electrodes were conducted as follows: The active material (NiO/Ni, NiO), carbon black and PVDF were added to NMP solvent as a slurry with a weight ratio of 8:1:1, respectively, and then the slurry was spread evenly on a Cu foil and baked at 80 °C in an oven for 16 hours. In addition, the Cu foil loaded with the active material was then punched to make a disc with a radius of 1 cm, and the loading amount per disc was approximately 1.5 mg. The prepared disc was assembled into a coin cell (2032) in an argon-filled glovebox using lithium metal as the counter electrode, Celgard 2250 as the battery separator, and the electrolyte was 1.0 M $LiPF_6$ (consisting of ethylene carbonate and diethyl carbonate at a weight ratio of 1:1). A constant current charge and discharge test of the assembled battery was performed on a NEWARE CT3008 multichannel battery measuring device. The test voltage range was 3-0.01 V (vs. Li/Li^+).

3. RESULTS AND DISCUSSION

The Ni-based precursor was obtained by the coprecipitation reaction between HMT, $Ni(NO_3)_2$ and $H_2C_2O_4$. It consists of $NiC_2O_4 \cdot 2H_2O$ cores and $Ni(OH)_2$ petal-like shells containing HCHO molecules[37]. The NiO/Ni composite was prepared by calcining the Ni-based precursor in an Ar atmosphere. The following reactions may have occurred during this process[36]:

$2HCHO(g) + 3Ni(OH)_2(s) \rightarrow 3Ni(s) + 5H_2O(g) + CO(g) + CO_2(g)$ (1)

$Ni(OH)_2(s) \rightarrow H_2O(g) + NiO(s)$ (2)

$CO(g) + NiO(s) \rightarrow CO_2(g) + Ni(s)$ (3)

$NiC_2O_4(s) \rightarrow 2CO_2(g) + Ni(s)$ (4)

To better understand the two prepared materials, their structures and morphologies were characterized by SEM, TEM and HRTEM. As shown in the SEM image of the NiO sample (Fig. 1a), the prepared NiO sample is very uniform with a flower-like morphology. Each flower-like particle with a diameter of approximately 1-2 μm is made up of many nanosheets. Fig. 1b shows the SEM images of the NiO/Ni composite. There is not much difference between the NiO/Ni composite and the NiO sample except that there are some tiny particles on the nanosheet of the NiO/Ni composite. Fig. 1c shows the TEM image of the NiO sample, and the inset of Fig. 1c shows the HRTEM image of NiO. The lattice fringes of 0.209 nm and 0.242 nm correspond to the 200-plane and 111-plane of NiO, respectively, which shows that the NiO sample was prepared successfully. Fig. 1d is the TEM image of the NiO/Ni composite, which differs from Fig. 1c. There are many granular materials (as shown by the direction of the arrows) on the nanosheet of the NiO/Ni composite. The inset of Fig. 1d shows that the lattice fringes of these particles correspond to the 111 facets of Ni metal. These results indicate that these Ni particles are embedded in the NiO nanosheets and that the preparation of the NiO/Ni composite was successful.

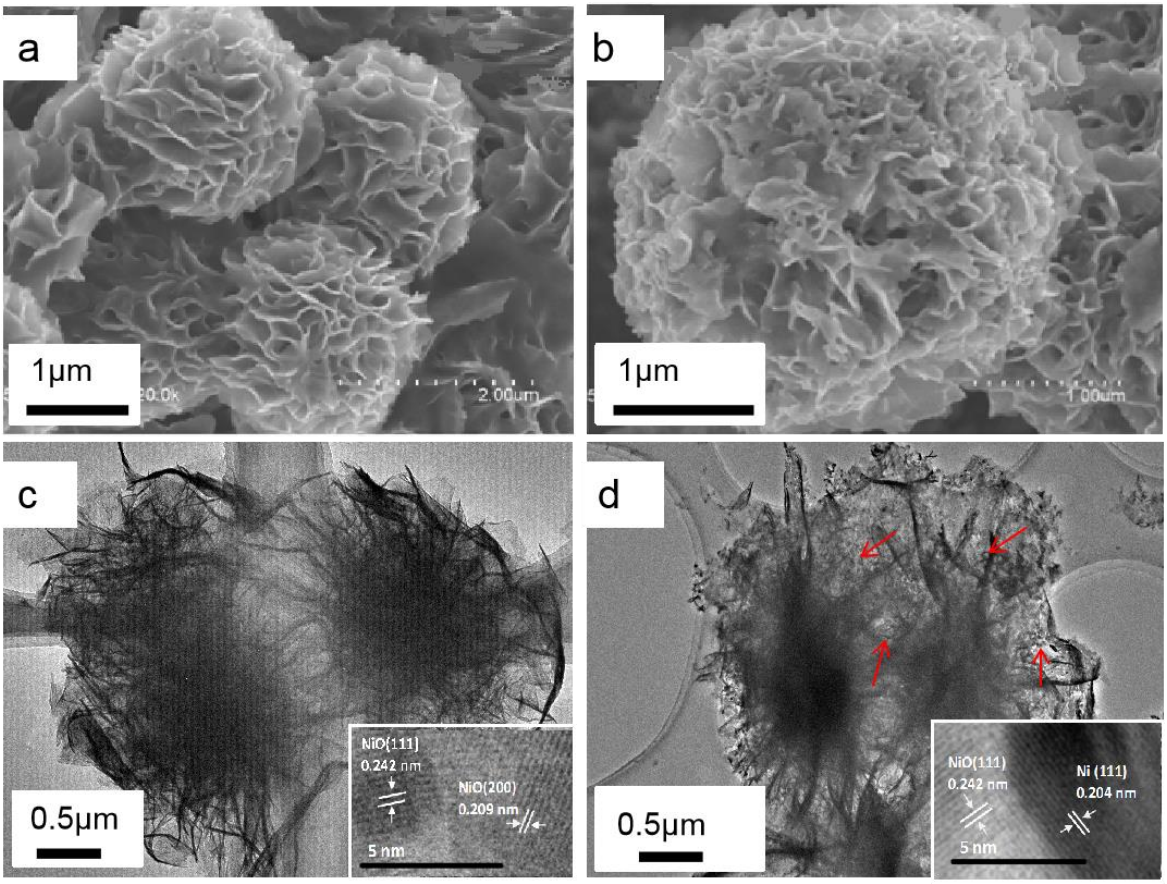

Figure 1. SEM images of (a) NiO and (b) NiO/Ni, TEM and HRTEM (insets) images of (c) NiO and (d) NiO/Ni.

To further confirm that the prepared material was NiO/Ni, phase analysis of the NiO/Ni composite, the NiO sample and pure metal Ni was carried out by XRD. Fig. 2 shows the XRD patterns of the NiO/Ni composite, the pure NiO sample, and pure Ni. It clearly shows that the first, second and fifth diffraction peaks of the NiO/Ni composite correspond to the diffraction peaks of NiO. The third, fourth and sixth diffraction peaks of the NiO/Ni composite correspond to the diffraction peaks of Ni. This result confirms that the NiO/Ni composite was prepared successfully by thermal decomposition of Ni-based precursors.

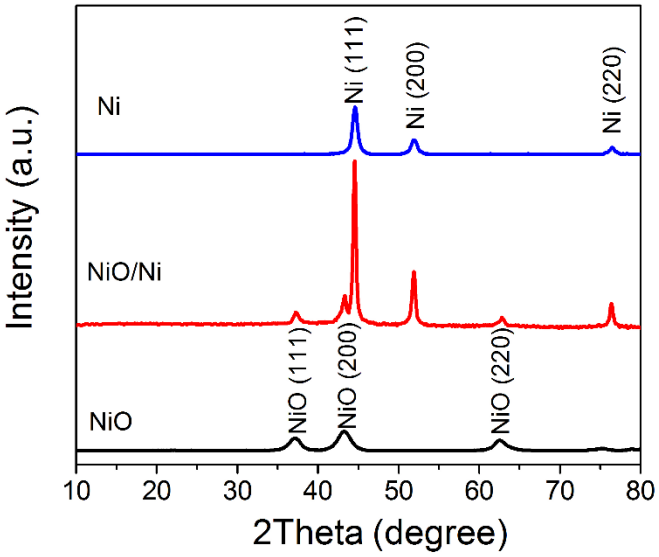

Figure 2. XRD patterns of Ni, NiO and NiO/Ni.

A thermogravimetric (TG) analyser was used to determine the content of NiO in the NiO/Ni composite. Fig. 3 shows the thermogravimetric analysis of the NiO/Ni composite and the calculated results. It can be seen clearly from the TG curve that the mass loss of the NiO/Ni composite is 11.3% between 100 °C and 400 °C. The process corresponds to the decomposition of NiO with the loss of O. The calculated result indicates that the NiO content in the NiO/Ni composite is 52.7%.

Table 1. The contents of Ni/NiO.

Sample	TG	
	NiO (%)	Ni (%)
Ni/NiO	52.7	47.3

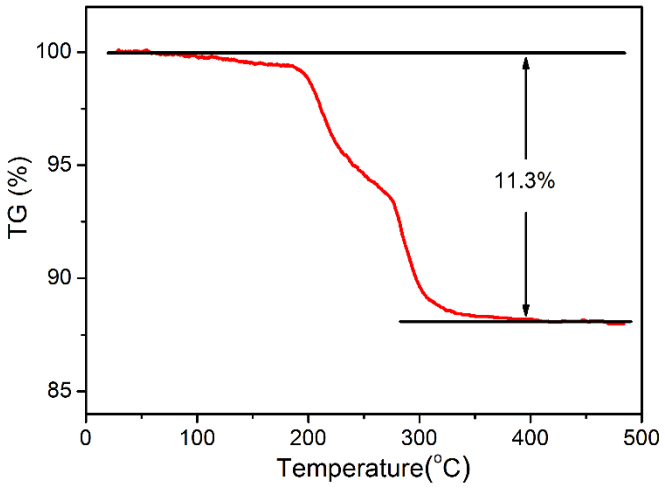

Figure 3. TG curve of NiO/Ni.

Fig. 4a and 4b present the dQ/dV curves of the NiO/Ni composite and the NiO sample, respectively. As shown in Fig. 4a, a strong reduction peak at 0.6 V in the first cycle corresponds to the initial reduction reaction of NiO to Ni^0 along with the formation of amorphous Li_2O and electrolyte decomposition to form the solid electrolyte interface (SEI) layer[31-32,37-38]. The composition of the SEI layer includes Li_2CO_3, ethyleneoxide-based oligomers, LiF, and lithium alkyl carbonate ($ROCO_2Li$)[39-40]. For the two subsequent cycles, as a consequence of the activation of the materials, the reduction peaks shifted to approximately 1.2 V and almost coincided. The areas under the curves of the second and third cycles are smaller than that of the first cycle, and the decreased area is attributed to the irreversible specific capacity. The two distinct oxidation peaks at approximately 1.4 and 2.1 V are observed in different cycles. The peak at approximately 1.4 V is due to the dissolution of the organic SEI layer. The peak at 2.1 V is ascribed to the decomposition of Li_2O and the oxidation of Ni^0 to NiO. These results are consistent with previous reports[32,38-39,41]. The changing trend and the locations of the peaks of the NiO sample are consistent with those of the NiO/Ni composite. As shown in Fig. 4a and 4b, the area enclosed by the NiO sample decreases more quickly than that of the NiO/Ni composite. This proves that the addition of Ni to the NiO/Ni composite enhances the conductivity of NiO and raises the effective content of NiO during the reaction. The reactions involved is:

$$NiO + 2Li^+ + 2e^- \leftrightarrow Ni(0) + Li_2O$$

The constant current charge-discharge test is one of the most important evaluations for lithium-ion battery electrode materials. A good electrode material usually has an obvious charge-discharge curve plateau. Fig. 4c and 4d show the charge-discharge curves of the NiO/Ni composite and NiO sample, respectively, for the 1st, 2nd, 10th and 30th cycles at a current density of 0.5 A g^{-1}. For the NiO/Ni electrode, the two plateaus and a sloping voltage range during the first discharge/charge are well coordinated. The narrow plateau at 1.5-0.6 V and a sloping region at 0.5-0.01 V during discharge correspond to the plateau at 1.2-1.6 V and the sloping region at 0.01-1.2 V during charging, demonstrating the formation and partial dissolution of the organic SEI layer, respectively. Meanwhile,

the long discharge peak at 0.5V and the charge peak at 2.1-2.5 V correspond to the reduction of NiO to metallic nickel along with the formation of amorphous Li_2O and its oxidation to NiO and decomposition of Li_2O[42]. These results are in agreement with the above dQ/dV results. Wang and co-workers have previously reported that the formation of the SEI layer had already started above 2.0 V during the first cathodic scan[43], and Tarascon and co-workers also observed the formation of the SEI layer by ex situ TEM in the sloping voltage range of 1 to 0.02 V[44]. In addition, Tu and co-workers reported that SEI layer formation started at a relatively high potential of 1.3 V, further grew at a lower potential of less than 0.5 V, and the formed SEI layer partially dissolved upon the subsequent charge.

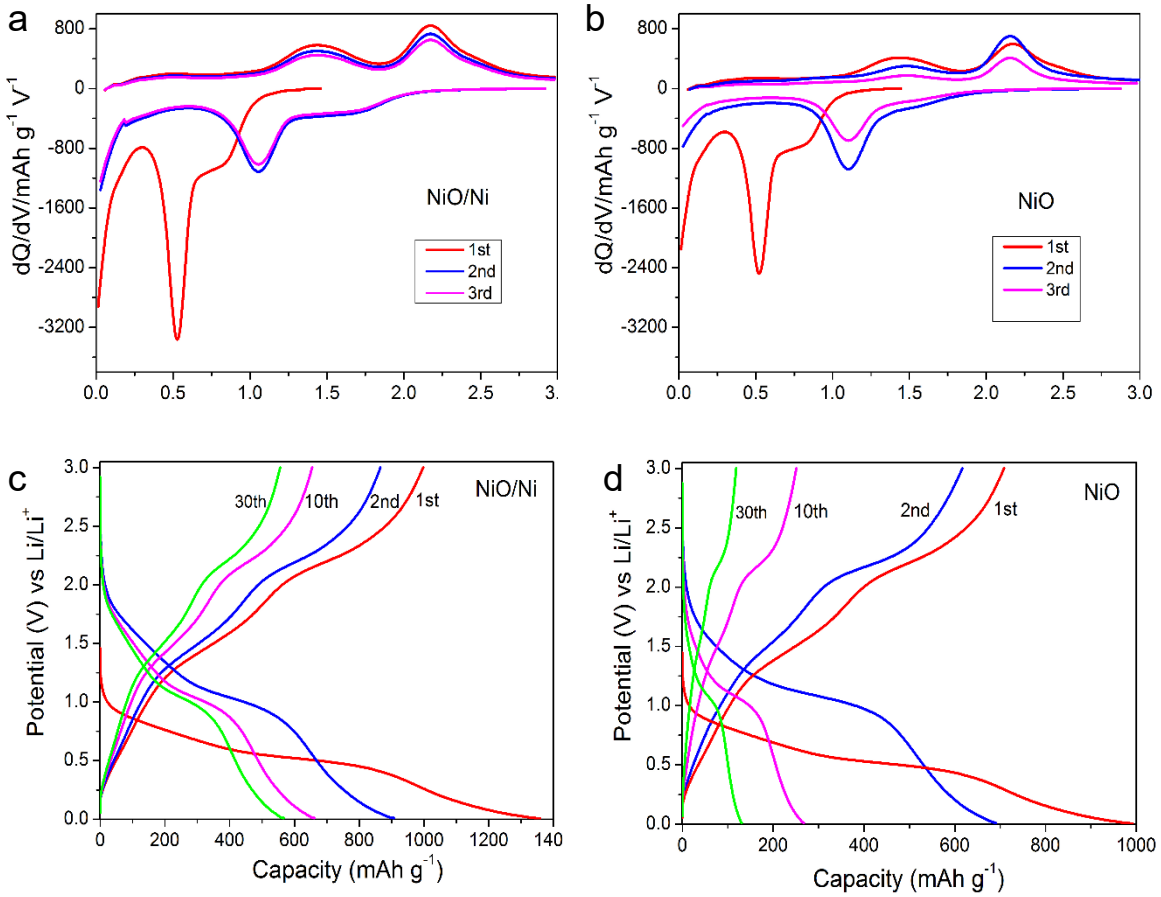

Figure 4. Charge and discharge curves for the first, second, 10th and 30th cycles of the (a) NiO/Ni composite and (b) NiO sample at a current density of 0.5 A g^{-1}; (c and d) the corresponding differential capacity (dQ/dV) vs. cell potential profiles.

These results indicated that Ni and Co nanograins of the composite can act as catalysts towards the formation/dissolution of the organic coating[42]. From Fig. 4c and 4d, it can be seen that the charge-discharge curves of the NiO/Ni composite and the NiO sample all have similar gradient charging-discharging platforms. The capacity of the NiO sample is much smaller than that of the NiO/Ni composite. The first discharge capacity of the NiO/Ni composite is much higher than that of the NiO sample (707 mAh g^{-1}), and the difference between the two is 290 mAh g^{-1}. This result also

demonstrates that the addition of Ni to the NiO/Ni composite improves the conductivity of NiO and increases the effective content of NiO during the reaction. The major potential peak of the NiO/Ni composite shifts to ~1.2 V during the following cycles, which may be related to the structural rearrangement.

Fig. 5a displays the rate performance of the NiO/Ni composite and the NiO sample as the anode at different current densities. The variation regularity of the rate performance for the two materials is almost the same except for an obvious difference in the amount of change when they are fully charged at different current densities. The discharge capacities of the NiO/Ni composite are 671.2, 460.3, 376.1, 344.9 and 555.8 mAh g^{-1} at current densities of 0.5, 1, 2, 4 and 0.5 A g^{-1}, respectively. This explains why the NiO/Ni composite can endure a high charge-discharge current density. Moreover, the charge and discharge capacities of the NiO/Ni composite are higher than those of the NiO sample at different current densities. The reason may be that the addition of elemental Ni in the NiO/Ni composite improves the conductivity of the material. Good conductivity benefits the quick release of the electrons generated during the redox reaction. More NiO in the NiO/Ni composite can participate in the electrochemical reaction. Fig. 5b shows the cycle performance of the NiO/Ni composite and the NiO sample at a current density of 0.5 A g^{-1}. The capacities of the NiO/Ni composite and the NiO sample all decrease significantly during the initial 15 cycles. However, the capacity of the NiO/Ni began to level off first. The capacities of the two electrodes gradually increase after the 40th cycle until the 100th cycle. The increasing capacity may be attributed to the reversible growth of a polymeric gel-like layer coming from kinetically activated electrolyte degradation and interfacial lithium storage[32]. Finally, the electrode of the NiO/Ni composite maintains a discharge capacity of 631.2 mAh g^{-1} after 100 cycles, which is significantly higher than that of the NiO sample (183 mAh g^{-1}). The result also proves that the addition of Ni metal not only increases the effective utilization of NiO in the NiO/Ni composite but also stabilizes the structure of the composite.

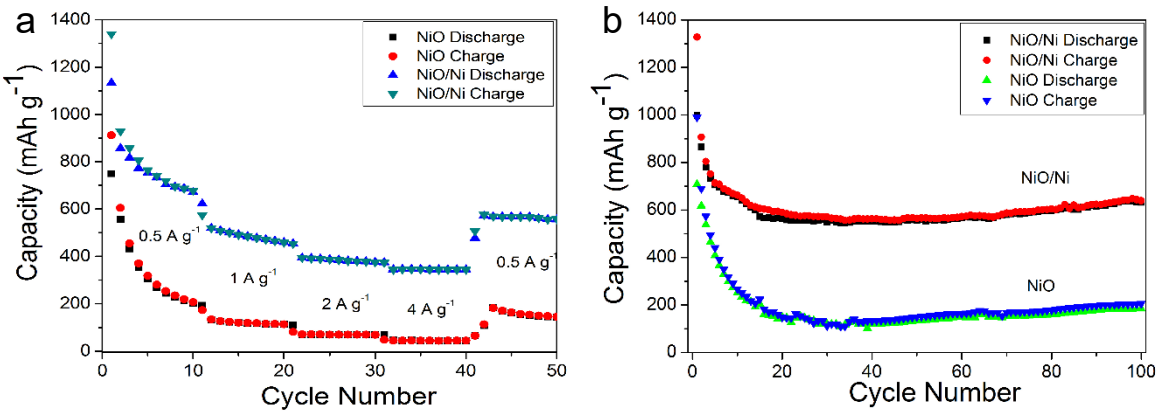

Figure 5. (a) Rate performance at various current densities and (b) cycle characteristics at a current density of 0.5 A g^{-1} of NiO/Ni composite and NiO sample.

To compare the cycle performance in this work with the previously reported data for NiO-Ni electrodes, we performed a literature survey, and the results are summarized in Table 2. The specific capacity of NiO/Ni is equivalent to or slightly better than that of most of the listed materials. This positive result can be explained by the NiO/Ni having a stable flower-like structure consisting of sheet-like NiO and granular Ni.

Table 2. Comparison of the electrochemical performances of Ni-NiO electrodes

Electrode	Current (m A g-1) 1C~718 m A g-1	Cycle Number	Reversible Capacity (mAh g-1)	References
NiO-Ni	718(1C)	100	264	45
NiO-Ni	286(0.4C)	50	397	46
NiO-Ni	143.6(0.2C)	30	520	43
NiO-Ni	359(0.5C)	100	627	47
NiO-Ni	215.4(0.3C)	70	669	48
NiO-Ni	107.7(0.15C)	100	704	49
NiO-Ni	156	65	646	50
NiO-G-Ni	125	150	722	51
NiO/Ni	500	100	631.2	This work

4. CONCLUSIONS

In summary, a NiO/Ni composite was obtained by thermal decomposition of a Ni-based precursor in an argon atmosphere. As a comparison, a pure NiO sample was obtained by thermal decomposition of the Ni-based precursor in air. The prepared NiO/Ni composite was shown to have a flower-like structure and consist of pure sheet-like NiO and pure granular Ni by SEM, HRTEM, TEM, and XRD. The thermogravimetric analysis showed that the NiO content in the NiO/Ni composite is 52.7%. As the anode of a lithium-ion battery, the NiO/Ni composite demonstrates a high discharge capacity of 555.8 mAh g^{-1} at a current density of 0.5 A g^{-1} after ten cycles of different current densities of 0.5, 1, 2, and 4 A g^{-1}, respectively. It shows outstanding charge-discharge rate performance, and it has a long cycle life with a 613.2 mAh g^{-1} discharge capacity after 100 cycles. The performance of the NiO/Ni composite was much better than that of the pure NiO sample. This may be due to the additional metallic Ni in the NiO/Ni composite, which improves the electrical conductivity of the composite, stabilizes its structure and increases the effective utilization of NiO in the NiO/Ni composite. The results indicate that the NiO/Ni composite is a favourable candidate for use as an anode material in lithium-ion batteries.

ACKNOWLEDGMENT
This work was supported by the Science and Technology Project of Guizhou Province [2018]1086.

CONFLICTS OF INTEREST
The authors declare no conflicts of interest.

References

1. H.H. Zhang, Z.G. Zou, S.C. Zhang, J. Liu, S.L. Zhong, *Int. J. Electrochem. Sci.*, 15 (2020) 12041.
2. C.Y. Zhu, Y.N. Zhang, X.H. Yu, P. Dong, J.G. Duan, J.M. Liu, J.X. Liu, Y.J. Zhang, *ChemSusChem*, 13 (2019) 803.
3. C.Y. Zhu, J.X. Liu, X.H. Yu, Y.J. Zhang, P.Dong, X. Wang, Y.N. Zhang, *Ceram. Int.*, 145 (2019) 19351.
4. Q.F. Zhao, S.Q. Zhang, C. Wang, G.H. Jiang, M.Y. Hu, Z.Y. Chen and Q.S. Ouyang, *Int. J. Electrochem. Sci.*, 16 (2021) 21053.
5. G.H. Jiang, Y.N. Zhang, Q. Meng, Y.J. Zhang, P. Dong, M.Y. Zhang, X.Yang, *ACS Sustainable Chem. Eng.*, 44 (2020) 18138.
6. Y.X. Fu, X.Y. Pei, D.C. Mo, S.S. Lyu, *J. Mater. Sci.: Mater. Electron*., 30 (2019) 5092.
7. H.H. Ru, K.X. Xiong, W. Zhou, Y.R. Zhu, X.S. Zhao, H. Chen, *Electrochim. Acta*, 222 (2016) 551.
8. C.M. Wang, H.L. Zhao, J. Wang, J. Wang, P.P. Lv, *Ionics*, 19 (2013) 221.
9. Q. X. Zeng, G. C. Xu, L. Zhang, H. Lin, Y. Lv, D. Z. Jia, *New J. Chem.*, 42 (2018) 7016.
10. Y.F. Liu, L.Q. Xiong, P.X. Li, H.Y. Fu, Z.C. Hou, L. Zhu, W.Z. Li, *J. Power Sources*, 428 (2019) 20.
11. Q.M. Su, S.X. Wang, Y.L. Xiao, L.B. Yao, G.H. Du, H.Q. Ye, Y.Z. Fang, *J. Phys. Chem. C*, 121 (2017) 3295.
12. S. Petnikota, H. Maseed, V.V.S.S. Srikanth, M.V. Reddy, S. Adams, M. Srinivasan, B.V.R. Chowdari, *J. Phys. Chem. C*, 121 (2017) 3778.
13. W. Wu, Y.S. Wei, H.J. Chen, K.Y. Wei, Z.T. Li, J.H. He, L.B. Deng, L. Yao, H.T. Yang, *J. Mater. Sci. Technol.*, 75 (2021) 110.
14. J.Z. Guo, S.H. Wang, X.H. Sun, R.S. Guo, K.Z. Xiong, R. Ling, K. Shen, J.H. Cui, H.Y. Ma, J. Zhou, S. Cai, J.F. Sun, *Ceram. Int.*, 47 (2021) 15743.
15. H.L. Yang, Y.S. Ye, Z.M. Wang, Z.H. Zhang, Y.L. Zhao, F. Yang, Z.Y. Zhu, T. Wei, *ACS Omega*, 5 (2020) 26230.
16. B.Y. Wang, Y.T. Xia, Z.W. Deng, Y. Zhang, H. Wu, *J. Alloys Compd.*, 835 (2020) 155239.
17. J. Long, Z.H. Yang, F.H. Yang, J. Cuan and J.X. Wu, *Electrochim. Acta*, 344 (2020) 136155.
18. Z.F. Zhang, X.M. Zhang, X.L. Liu, W.Q. Zhang, Y.G. Zhang, Y.Y. Li, C.L. Qin, W.M. Zhao, Z. Bakenov, *Chem. Eng. J.*, 388 (2020) 124207.
19. H.J. Shin, J.Y. Hwang, H.J. Kwon, W.J. Kwak, S.O. Kim, H.S. Kim, H.G. Jung, *ACS Sustainable Chem. Eng.*, 8 (2020) 14150.
20. L. Tong, P. Wang, A.R. Chen, F. Qiu, W.Z. Fang, J. Yang, C. Wang, Y. Yang, *Carbon*, 153 (2019) 592.
21. S.C. Guo, X. Hu, Y. Hou, Z. Wen, *ACS Appl. Mater. Interfaces.*, 9 (2017) 42084.
22. C.H. Hsu, H.Y. Chen, C.J. Tsai, *J. Power Sources*, 438 (2019) 226943.
23. W.J. Deng, X.S. Wang, C.Y. Liu, C. Li, M.Q. Xue, R. Li, F. Pan, *ACS Appl. Energy Mater.*, 1 (2018) 312.
24. M. Chamas, A. Mahmoud, J.L. Tang, M.T. Sougrati, S. Panero, P.E. Lippens, *J. Phys. Chem. C*, 121 (2017) 217.
25. J. Peng, W.C. Zhang, M.T. Zheng, H. Hu, Y. Xiao, Y.L. Liu, Y.R. Liang, *J. Colloid Interface Sci.*, 587 (2021) 590.
26. L. Cao, D.X. Wang, R. Wang, *Mater. Lett.*, 132 (2014) 357.
27. S.B. Ni, X.H. Lv, J.L. Ma, X.L. Yang, L.L. Zhang, *J. Power Sources*, 270 (2014) 564.

28. Y.L. Tan, Q. Li, Z. Lu, C.X. Yang, W.W. Qian, F.Y. Yu, *Electrochim. Acta*, 874 (2021) 159788.
29. T. Zhang, Y.Q. Sun, L.F. Hang, H.L. Li, G.Q. Liu, X.J. Lyu, W.P. Cai, Y. Li, *ACS Appl. Mater. Interfaces*, 10 (2018) 9792.
30. J. Bai, D.D. Gao, H.M. Wu, S.Q. Wang, F.Y. Cheng, C.Q.Feng, *J. Nanosci. Nanotechno.*, 19 (2019) 8063.
31. X.L. Sun, W.P. Si, X.H. Liu, J.W. Deng, L.X. Xi, L.F. Liu, C.L. Yan, O.G. Schmidt, *Nano Energy*, 9 (2014) 168.
32. Z.C. Bai, Z.C. Ju, C.L. Guo, Y.T. Qian, B. Tang, S.L. Xiong, *Nanoscale*, 6 (2014) 3268.
33. H. Liu, G.X. Wang, J. Liu, S.Z. Qiao, H.J. Ahn, *J. Mater. Chem.*, 21 (2011) 3046.
34. C.Y. Wu, H. Yang, C.Y. Wu, J.G. Duh, *J. Alloys Compd.*, 750 (2018) 23.
35. C.Y. Xiong, B.B. Li, W.H. Dang, W. Zhao, C. Duan, L. Dai, Y.H. Ni, *Mater. Des.*, 195 (2020) 108942.
36. H.W. Lai, Q. Wu, J. Zhao, L.M. Shang, H. Li, H. Guo, *Energy Environ. Sci.*, 9 (2013) 2053.
37. J.F. Xiong, H. Shen, J.X. Mao, X.T. Qin, P. Xiao, X.Z. Wang, Q. Wu, Z. Hu, *J. Mater. Chem.*, 22 (2012) 11927.
38. X.H. Wang, L. Qiao, X.L. Sun, X.W. Li, D.K. Hu, Q. Zhang, D.Y. He, *J. Mater. Chem. A*, 1 (2013) 4173.
39. S.H. Wang, Z.Y. Yuan, W.L. Wu, Y.L. Li, H.W. Mi, X.Z. Ren, P.X. Zhang, L.N. Sun, *J. Alloys Compd.*, 862 (2021) 158012.
40. X.H. Huang, J.P. Tu, X.H. Xia, X.L. Wang, J.Y. Xiang, L. Zhang, Y. Zhou, *J. Power Sources*, 188 (2009) 588.
41. X.Y. Yan, X.L. Tong, J. Wang, C.W. Gong, M.G. Zhang, L.P. Liang, *J. Alloys Compd.*, 556 (2013) 56.
42. Y.J. Mai, J.P. Tu, X.H. Xia, C.D. Gu, X.L. Wang, *J. Power Sources*, 196 (2011) 6388.
43. C. Wang, D.L. Wang, Q.M. Wang, H.J. Chen, *J. Power Sources*, 195 (2010) 7432.
44. S. Grugeon, S. Laruelle, R. Herrera-Urbina, L. Dupont, P. Poizot, J.M. Tarascon, *J. Electrochem. Soc.*, 148 (2001) A285.
45. M.A. Rahman, C. Wen, *Ionics*, 21 (2015) 2709.
46. X.F. Li, A. Dhanabalan, C.L. Wang, *J. Power Sources*, 196 (2011) 9625.
47. M. Morozov, S. Ivanov, M. Kadirov, A. Bund, *J. Appl. Electrochem.*, 51 (2021) 815.
48. J.C. Zhang, S.B. Ni, J. Tang, X.L. Yang, L.L. Zhang, *Mater. Lett.*, 176 (2016) 21.
49. S.B. Ni, X.H. Lv, J.J. Ma, X.L. Yang, L.L. Zhang, *J. Power Sources*, 270 (2014) 564.
50. X.F. Li, A. Dhanabalan, K. Bechtold, C.L. Wang, *Electrochem. Commun.*, 12 (2010) 1222.
51. X.L. Chen, T. Xiao, S.L. Wang, J. Li, P. Xiang, L.H. Jiang, X.Y. Tan, *Mater. Chem. Phys.*, 222 (2019) 31.